國立交通大學

材料科學與工程學系

奈米科技碩士班

碩 士 論 文

操控不鏽鋼奈米孔洞調控生物相容性與

成骨細胞功能表現

Control of biocompatibility and cellular function for osteoblasts

by tunable stainless steel nanostructure

研 究 生：謝 孟 哲

學號：9852520

指導教授：黃 國 華 教授

中 華 民 國 一 百 年 七 月

運用可控制得不鏽鋼奈米孔結構控制成骨細胞的生物相容性和細胞功能

Control of biocompatibility and cellular function for osteoblasts by tunable stainless steel nanostructure

研 究 生:謝孟哲　　Student: Meng-Je Shie

指導教授:黃國華　　Advisor: Dr. Guewha Steven Huang

國 立 交 通 大 學

材 料 科 學 與 工 程 學 系

奈 米 科 技 碩 士 班

碩 士 論 文

A Thesis

Submitted to Graduate for Nanotechnology

Deparment of Materials Science and Engineering

College of Engineering

National Chiao Tung University

in partial Fulfillment of the Requirements

for the Degree of

Master

in

Nanotechnology

July 2011

Hsinchu, Taiwan, Republic of China

中華民國一百年七月

誌　謝

時間過得很快，兩年的碩士生活一下子就過了。我很慶興能夠進入奈米所跟隨 黃國華教授的研究團隊一起學習成長。教授總是很認真仔細的關心我們的研究進度並給予我們寶貴的建議，就算周末假日也來學校和我們一起奮鬥，真的是花飛無數的心血在我們身上。除了生物方面的專業知識以外，教授也給了我們很多人生經歷的建議。教授總是會和我們分享他所看見的人事物以及重要的國際觀以及人生觀，讓我的態度更加成熟穩重也因此我才能順利獲得台積電的工作機會。

在碩士生活中除了感謝日以繼夜、焚膏繼晷指導我們的 黃國華教授以外，也很感謝師母 洪孟燕 女士，師母總是會準備很多營養好吃的食物來慰勞我們，在於實驗室的重大活動上也不虞心力得參與和我們一起奮鬥。師母具有很多社會歷練給我們的建議都考慮了非常多層面，讓我們學習到做事不只要看表面還要用有遠見。也很感謝 洪耀欽 醫師常常關心我的實驗以及生活狀況，在我研究不順和興情不愉快的時候洪醫師總是給我多的關懷。洪醫師總是會向爸爸一樣得幫我加油打氣給我鼓勵使我能夠再次振作面對困難，也總是出資讓我們研究團隊聚餐辦活動聯絡感情，真得是很感謝洪醫師的關懷。

還有要感謝實驗室的伙伴們，敘安學長總是很有耐性的和我討論

實驗給我建議，實驗研究方法都是敘安學長一步一步的帶我一步一步做出來的。我是物理背景的對生物一竅不通總是給他帶來很多麻煩，都是敘安學長耐心的帶領下才能將研究完成，真的很感謝他。大勳學長幫助我完成了不鏽鋼得製成，即使在當兵也常常打電話關心我的狀況，在我遇到困難也不遺餘力的幫我借儀器給我意見，只可惜他當兵和他只有一年的相處時間，真的很感謝大勳學長給我的幫助。嘉惠學姐總是不厭其煩得跟我講解一些生物的知識，百忙之中還是很有耐心的回答我的問題給我建議，在我心情低落的時候也總是幫我加油打氣，平常總是提醒神經大條得我很多細節讓我避免犯錯，甚至幫助大家敬形很多的困難實驗，很感謝學姐這兩年來的幫助和關懷，讓我順利得度過碩士生活。還實驗室的同學們和學弟學妹總是一起熬夜一起奮鬥互相幫忙互相扶持。

最後要感謝我的爸爸媽媽姑姑等家人給我資源上資助讓我免於挨餓受凍夜給了我很多的關懷和幫助以及中興物理的伙伴們幫我加油打氣讓我的碩士生涯充滿活力。感謝大家的幫忙，沒有你們就沒有今天的謝孟哲

操控不鏽鋼奈米孔洞調控生物相容性與成骨細胞功能表現

學生:謝孟哲　　指導教授:黃國華 教授

國立交通大學材料科學與工程學系奈米科技碩士班

碩士論文

摘　　要

運用陽極氧化過程製造的奈米孔洞在生物醫學應用上已經受到相當大的關注。之前的研究已經證明相較於沒有陽極氧化製做結構的部分，奈米孔洞可以促進成骨細胞的貼附以及功能性的發展。最近一項研究發現奈米孔洞的直徑可以決定細胞得發展。不鏽鋼的材質對於骨頭生長擁有很多的好處相較於其他材料，因此有越來越多的需求探討成骨細胞在不鏽鋼材質的奈米孔洞表面上的生長。基於這個原因，我們對成骨細胞在不同尺寸的不鏽鋼奈米孔洞上的行為進行探討。細胞的形態，生存能力，貼附和礦化現象將被探討。

結果顯示直徑 40 奈米和 100 奈米對於細胞的形態，生存能力，貼附，鹼性磷酸酶活性和礦化現象有很好的影響。在細胞型態和生存能力上 40 奈米和 100 奈米有很好的表現，在 40 奈米上細胞的貼附和骨架發展得最好。而礦化發生的效率在 40 奈米到 100 奈米之間隨者孔洞半徑得上升而上升。這些現象可能是因為奈米孔洞在奈米尺寸下不同的粗糙度引發的。我們的研究顯示奈米型態的表面對於成骨細胞功能性的協同作用並可應用於設計更好的生醫植入物表面。

Control of biocompatibility and cellular function for osteoblasts by tunable stainless steel nanostructure

Student: meng-je Shie Advisor: Dr. Guewha Steven Huang

Graduate for Nanotechnology
Deparment of Materials Science and Engineering
National Chaio Tung University

ABSTRACT

Nanopore layers by anodization have received considerable attention in biomedical application. Previous studies have demonstrated increased osteoblast (bone-forming cell) adhesion and function on nanopore layers compared with unanodized counterparts. More recently, one study showed nanopore diameter determined cell fate. The stainless steel material is known to be much more beneficial for bone growth than others material, so there is increasing demand to explore the response of osteoblast on stainless steel with nanopore layer. For this reason, we evaluated MG63 osteoblast behavior on different diameter nanopore layers with stainless steel. Cell morphology, viability, adhesion and mineralization were evaluated.

The results showed that the diameter of 40nm and 100nm provided an effective length scale for cell morphology, viability, focal adhesion,

alkaline phosphatase activity, and mineralization. The cell morphology and viability showed good expression on 40nm and 100nm, best adhesion and actin filament occurred at 40nm. The mineralization rates of cells cultured on stainless steel nanopore layers increased with increasing pore diameter from 40 to 100 nm, which may be attributed to different length and nanometer-scale roughness of the nanotube layers.

Our study reveals a synergistic role played by the nanotopographies in osteoblast functions and provides insight to the design of better biomedical implant surfaces.

Introduction

It is well known that the surface characteristics and topology of biomedical implants play critical roles in cell or extracellular matrix interactions with the implants. The surface material plays primary role in controlling cellular behaviors, such as focal adhesion [1-3]. Metals and alloys are the most common materials used as surgical implants, such as cobalt-chromium alloys, tantalum (Ta), niobium (Nb) and titanium (Ti) have been used for implants, since they have excellent corrosion resistance[4]. Cytotoxicity is often dependent on the ionization tendency of the metals used, and the biocompatibilities of refractory metals are evaluated [4].Stainless steel in particular show properties which make them suitable as surgical implant materials[5-16]. It has been suggested that microtopographies can promote bone-to-implant contact via such mechanisms as mechanical interlocking[17] and enhancement of osteoblast functions by these microtopographies[18, 19], such as nanorod[20, 21], grooves[22], nanodot[23], nanoflower[24]. In addition, cells are also grown on random structures such as nanofibers[25] or metal surface[26]that mimic active structure of extracellular matrix.

The interactions between cells and nanotopographies are of increasing interest as a nanotopographies may be more efficient in promoting cell functions[27] and nanotubes have attracted much attention[28-39]. Nanotubes with the suitable tube dimensions have been observed to enhance bone cell functions[28-37, 40, 41], even though there is still some controversy. These nanotubes can also serve as carriers for drugs such as growth factors[37, 38, 42], antibacterial agents[29, 33] and other drugs[38] and show promise in bone implant applications.

Bone tissues are composed of nanostructures including non-collageneous organic proteins, fibrillar collagen and hydroxyapatite crystals, microstructures including lamellae, osteons and Haversian systems, as well as macrostructures such as cancellous and cortical bones[43]. From the biomimetic viewpoint, a hierarchical structure composed of microand nanoscale components may provide a more suitable surface topography for cell functions as it can better mimic the structure of the natural extracellular matrix. There have been some attempts to fabricate such micro/nanostructures for biomedical applications such as tissue engineering scaffold, implant surfaces.

In this study, nanoscaled periodic surface structures were generated

on medical stainless steel AISI 304L stainless steel and their influence on osteoblastic cells was observed. We fabricated nanpore on stainless steel surface by anodization, the pore size of stainless steel is controllable and uniformly distributed; the diameter of pores depends on the voltage applied. The current study is based on hypothesis that nanotopography may modulat and control the growth, proliferation and biological function of osteoblast and nanopore have attracted much attention. The templates that nanopore nanostructure fabricated on stainless steel have good biocompatibility. It could serve as a convent platform to optimize the bone-implant interface. Association of nanopography with clinical outcome will be investigated and discussed.

Experimental Methods

1.1 Cell culture

To eliminate possible contamination of nano-micro particles, the cell culturing was performed in a class-10 clean room. MG63 cells were cultured in Dulbecco's Modified Eagle's Medium complimented with 10% FBS and incubated at 37 ℃, 5% CO_2.

1.2 Chemicals

Glutaraldehyde and osmium tetroxide were purchased from Electron Microscopy Sciences (USA). Anti-vinculin mouse antibody was purchased from Abcam (USA). Alexa Fluor 594 phalloidin, Alexa Fluor 488 goat anti-mouse IgG, were purchased from Invitrogen (USA). Trypsin was purchased from Sigma (USA). Bromodeoxyuridine drug and antibody were purchased from Millipore. Other chemicals of analytical grade or higher were purchased from Sigma or Merck.

1.3 Fabrication of nanopore arrays

The 304L stainless steel samples were rather thick (25mm×25mm×2mm) with a thread for the electrical contact. This austenitic polycrystalline steel contains (w%): Cr: 18.68, Ni: 10.14, Mn: 1.72, Mo: 0.35, Cu: 0.15, N: 0.072, C: 0.018 and Fe balanced. The samples were mechanically polished with abrasive papers (grade 500, 1200, 2400 and 4000) followed by diamond pastes of decreasing grade (3, 1 and 0.25m). Between each polishing, they were rinsed with acetone, ethanol and distilled water under ultrasonic bath for 10min[44].

As soon as this mechanical polishing was achieved, electropolishing was performed in an electrolytic bath, whose temperature was maintained between −5 and 15 ◦C for 30 minutes. The electrolyte was composed of a mixture of 40mL of perchloric acid and 760mL of ethylene-glycol monobutylether. The perchloric acid was used to achieve the proper low pH for promoting the ionization of metallic atoms into metallic cations instead of oxides formation. The ethylene-glycol monobutylic ether ensures a high viscosity of the electrolyte.

Samples (anodes) were positioned vertically in front of the counter

electrode, which was a rectangular carbon cathode, by far larger than the anode . These two electrodes were linked up to a DC generator. This power supply provided either a control of the current intensity delivered at an imposed constant bias voltage or vice versa. The anodization applied voltages were 30 , 45 , 60 , 70 , 75 volt for 40 , 100 , 180 , 200 , 220 nm nanopores array, the electrolytic solution was stirred by a rotating magnet . After the electropolishing, the samples were rinsed with large amounts of distilled water, then cleaned during the electrolyte overnight.

The dimension and homogeneity of nanodot arrays were measured and calculated from images taken by JEOL JSM-6500 TFE-SEM.

1.4 The cells viability assay.

Cells were harvested and fixed with 4% paraformaldehyde in PBS for 30 minutes followed by PBS wash for three times. And membrane was permeated by incubating in 0.1% Triton X-100 for 10 min, followed by PBS wash for three times. The sample was incubated with 4',6-diamidino-2-phenylindole (DAPI) and phalloidin for 15 minutes at room temperature followed by PBS wash for three times.

1.5 Scanning electron microscopy (SEM)

The harvested cells were fixed with 1% glutaraldehyde in PBS at 4 ℃ for 20 minutes, followed by post-fixation in 1% osmium tetraoxide for 30 minutes. Dehydration was performed through a series of ethanol concentrations (10-min incubation each in 50%, 60%, 70%, 80%, 90%, 95%, and 100% ethanol) and air dried. The specimen was sputter-coated with platinum and examined by JEOL JSM-6500 TFE-SEM at an accelerating voltage of 5 k-electron voltage (eV).

1.6 Immunostaining

Cells were harvested and fixed with 4% paraformaldehyde in PBS for 15 minutes followed by PBS wash for three times. Membrane was permeated by incubating in 0.1 % Triton X-100 for 10 min, followed by PBS wash for three times, blocked by 1 % BSA in PBS for 1 hr, and PBS wash for three times. The sample was incubated with anti-vinculin antibody (properly diluted in 0.5 % BSA) and phalloidin for 1 hr, followed by incubating with Alexa Fluor 488 goat anti-mouse antibody for 1 hr followed by PBS wash for three times and examined by .

1.7 Alizarin Red S stain

The Mg63 cells on substrate were washed PBS and fixed with 4% paraformaldehyde for 10 min. After washed by DI water the fixed cells were soaked in 2% Alizarin Red s in DI water (adjusted to pH for 4.2) at 37 ℃ for 20 minute and washed with DI water to remaining stains. We randomly picked fifty cells for each condition and calculated the area of stain per cell relative to the area of stain per cell on flat surface.

1.8 Alkaline phosphatase(ALP) assay

Cultured MG63 were lysed in 1X lysis buffer (Tris-Cl (Ph 7.4), NaCl,EDTA, triton X-100, PMSF, proteinase inhibitor cocktail tablet (Roche), H2O) and scraped, and spun down at 12000 g for 2 mins at 4℃ . Then, the supernatants were removed andplaced into new Eppendorf tubes and we used UV/OD to define the proteins concentration. After we knew the proteins concentration we mixed 20µl sample buffer and 100 µl pNPP substrate solution then incubated in dark for 30 minutes. After the incubation period, read the plate at 405 nm on a multiwell plate reader.

II. Results and Discussions

2.1 Fabrication of nanopre arrays for the growth of MG63

Stainless steel plays an important role on biomedical applications, due to its corrosion resistance and excellent mechanical properties. Its scope of application ranges from clinical devices such as stents and artificial joints to surgical tools. One of the major tasks of biomaterial research is the functionalization of the material surface to improve the biocompatibility according to a specific application. To investigate the effect of the aspect ratio of the nanopore structure on cell behavior, various nanopore array surface consisting of nanopores that varied in diameter were fabricated[44].

Figure 1 A shows SEM images of stainless steel 304L nanopore layers fabricated by anodization in 5 wt % perchloric acid at different anodization voltage for 30 minute in − 5 and 15 ◦C. It is apparent from Figure 1 the diameter of nanotube layers is approximately 40, 100, 180, 200, and 220 nm under 30, 45, 60, 70, and 75 V. As shown in Figure 1 B,

this characteristic diameter increases linearly with the value of the applied voltage. Such a linear variation was also reported for anodic aluminium and titanium oxides.

(A)

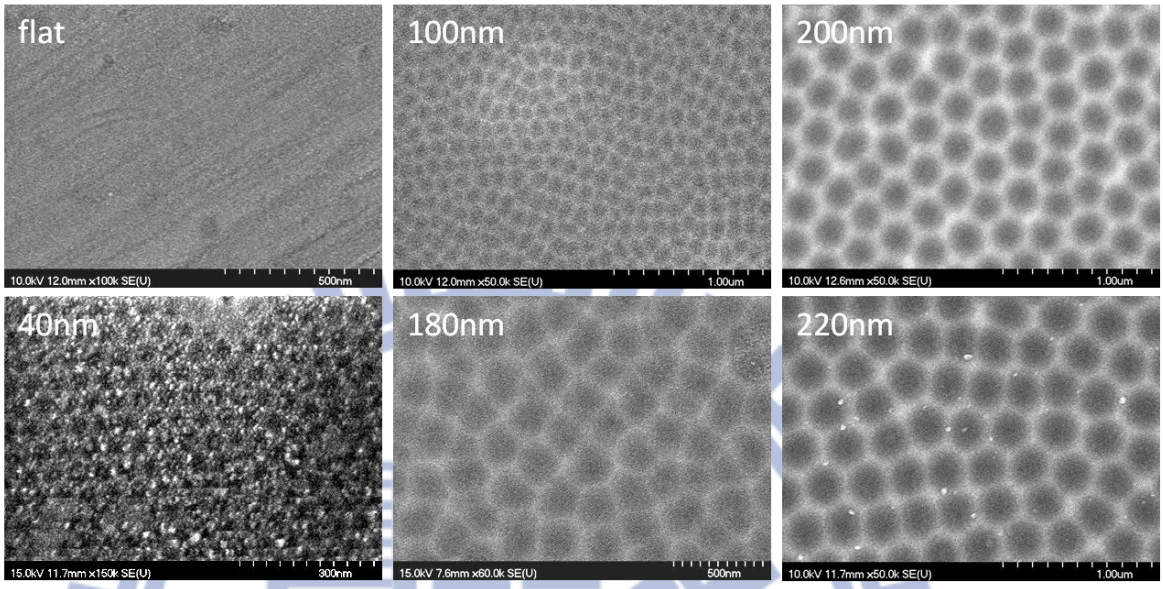

(B)

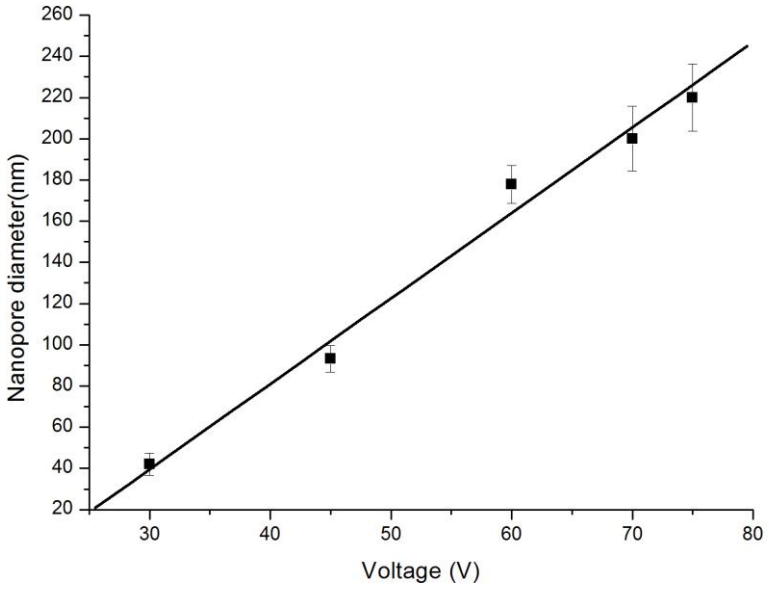

Figure 1. Stainless steel nanopore arrays were fabricated by AAO processing. (A) High resolution scanning electron micrographs of nanopore surface: Flat, 40-nm, 100-nm, 180-nm, 200nm and 220nm(B) the inter-pore distance increases linearly with bias voltage.

2.2 Nanotopography modulated cell viability and morphology of MG63

To evaluate the viability of osteoblast, MG63 were cultured on fabricated nanopore arrays and on flat stainless steel 304L at the density of 250 cells per square centimeter. Cell viability on the specimens during the 24 h (day 1), 72 h (day 3) and 120 h (day 5) of incubation is shown in Figure 2. Density of viable cells was obtained from composite pictures Figure 3 At each time interval adopted in this study, the adherent cell numbers on the each size of nanopore surfaces are larger than that on the smooth surface. The cell numbers are slight different between each size surface, the cell number on the 100nm nanopore surface is slightly higher than the other size surfaces on 24 hours. After incubation for 72 h and 120 h cell numbers on the 40nm and 100nm is obviously higher than on the 180, 200 and 220 nm nanopre array surface. On day 3 and day 5 cell numbers significant increase of growth was observed with cells grown on 100 nm and 40 nm nanopore array when compared to flat surface.

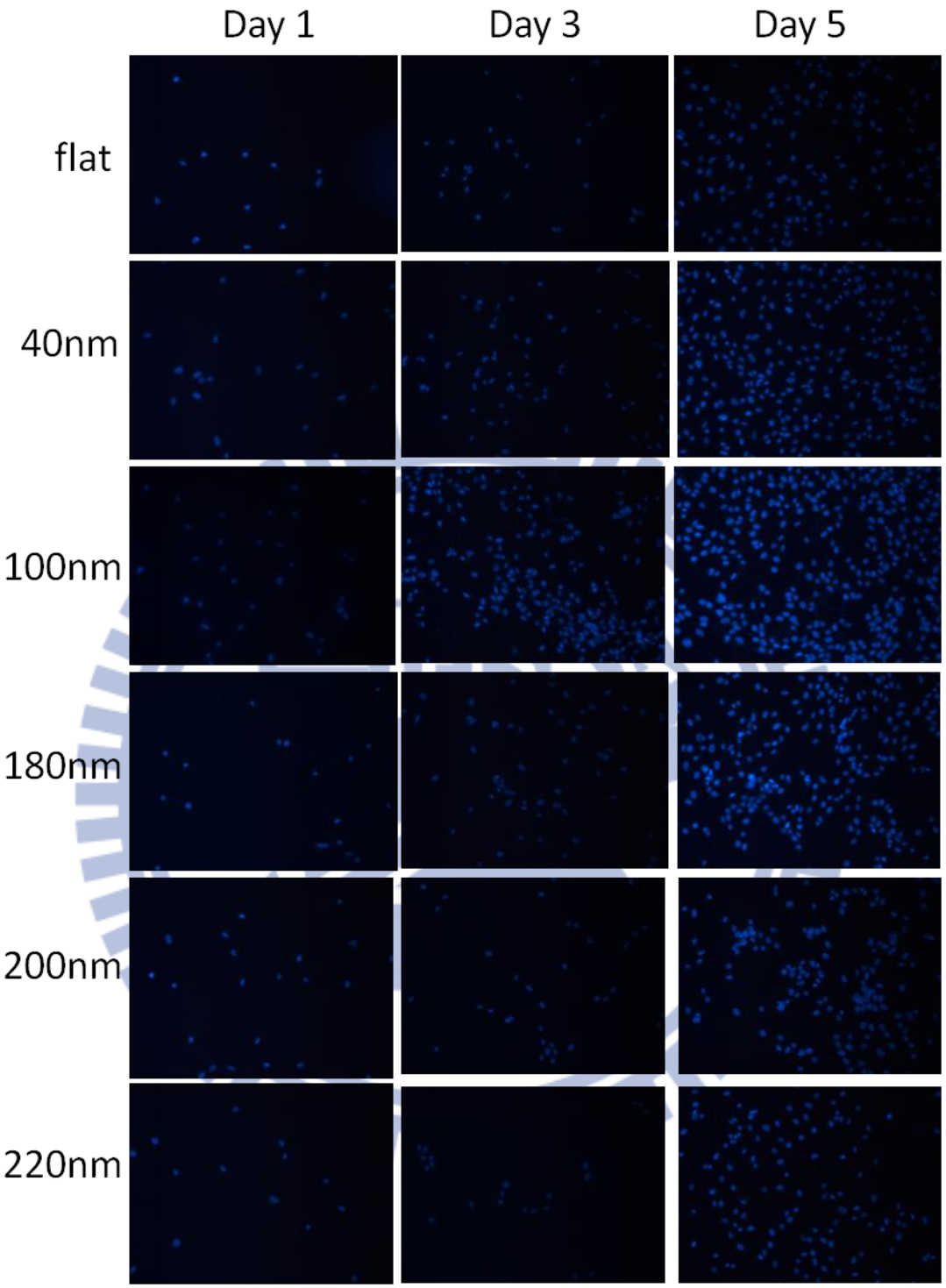

Figure 2.Immunostaining to show distribution of DAPI of osteoblast cultured on nanopore arrays. The cell were seeded on flat, 40 nm, 100 nm, 180 nm, 200 nm and 220 nm nanopore arrays.

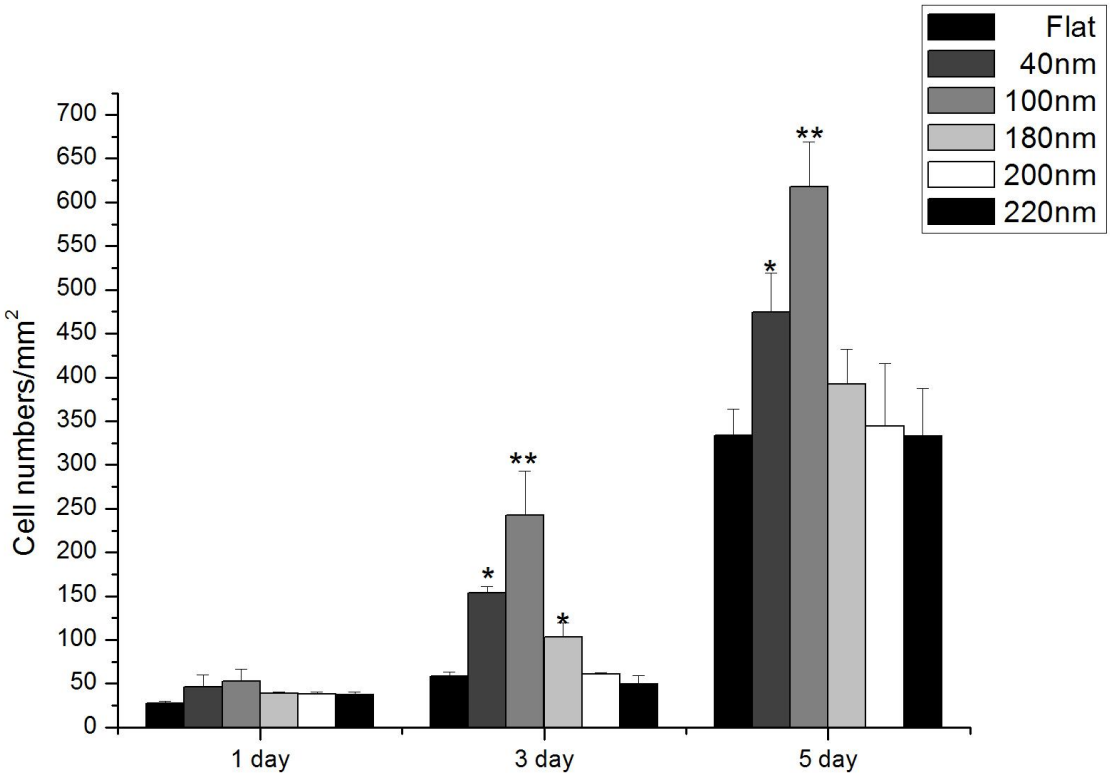

Figure 3.The cell density of osteoblasts grown on various sizes of nanopore arrays harvested on Day 1, 3, and 5. Cell density was derived from counting the number of cells stained by DAPI . * =TTEST , $p<0.005$

osteoblasts grown on various sizes of nanopore

Morphology is an important index for cell growth. Nanotopography is known to modulate cell morphology of MG63 cells. Biochemical and genetic evidence indicated that apoptosis occurs to cells with abnormal morphology.

In order to observe the morphology of Mg63 on stainless steel surface, MG63 osteoblast were cultured on fabricated nanopores and flat stainless steel at the density of 1000 to 1300 cells per square centimeter . Cells were harvest on day 1, 3 and 5 after seeding. SEM was performed to examine the morphology of cells(Figure 4). Surface area were measured and compared to cells grown on flat surface(Figure 5) Cell density on 100nm nanopore is higher than other size on day 1 and 3 , and there are slightly different between the other size .

There are minor differences on morphology for cell growth on different nanostructures. The variation of cell morphology was also dependent on incubating time. On day 1, cell surface area increase on 40nm than flat , cell area decreased with nanopore size increased. On day 3, significant increase of surface area increased was observed on 40nm and 180nm. On day 5, surface area increase on all size nanopore array than flat.

In summary, the higher cell density was observed on 100nm nanopoe array, and cell growth on 40nm nanopore exhibited better morphology in flatness and extend area. Maybe cell area decrease because high cell density on 100nm and day5.

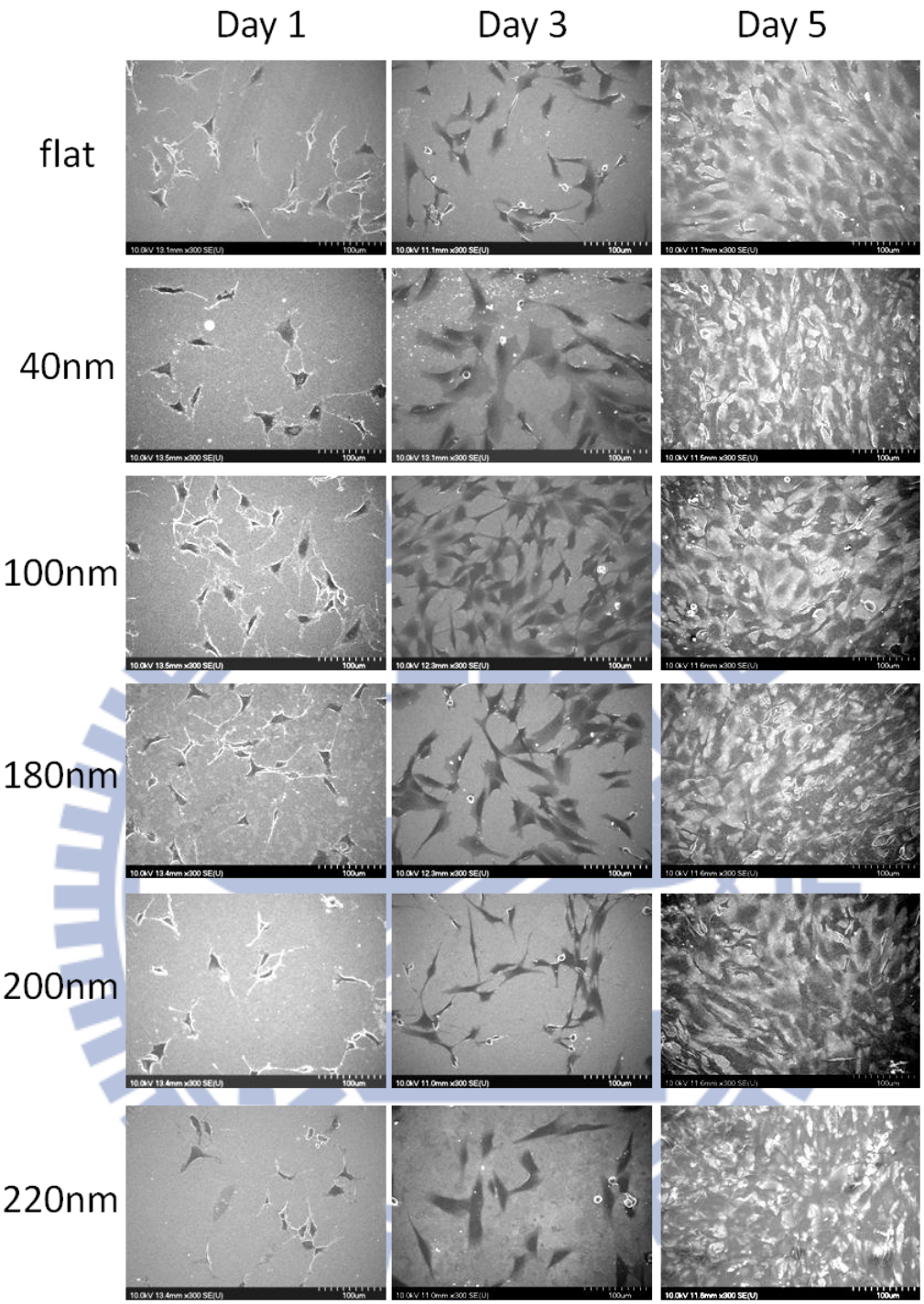

Figure 4.Morphology of MG63 osteoblast cultured on nanopore arrays. Mg63 cells were grown on Flat,10-nm,50-nm,100-nm,and 200-nm nanopore arrays for 1 day ,3 days, and 5 days and their morphology imaged by scanning electron microscopy.

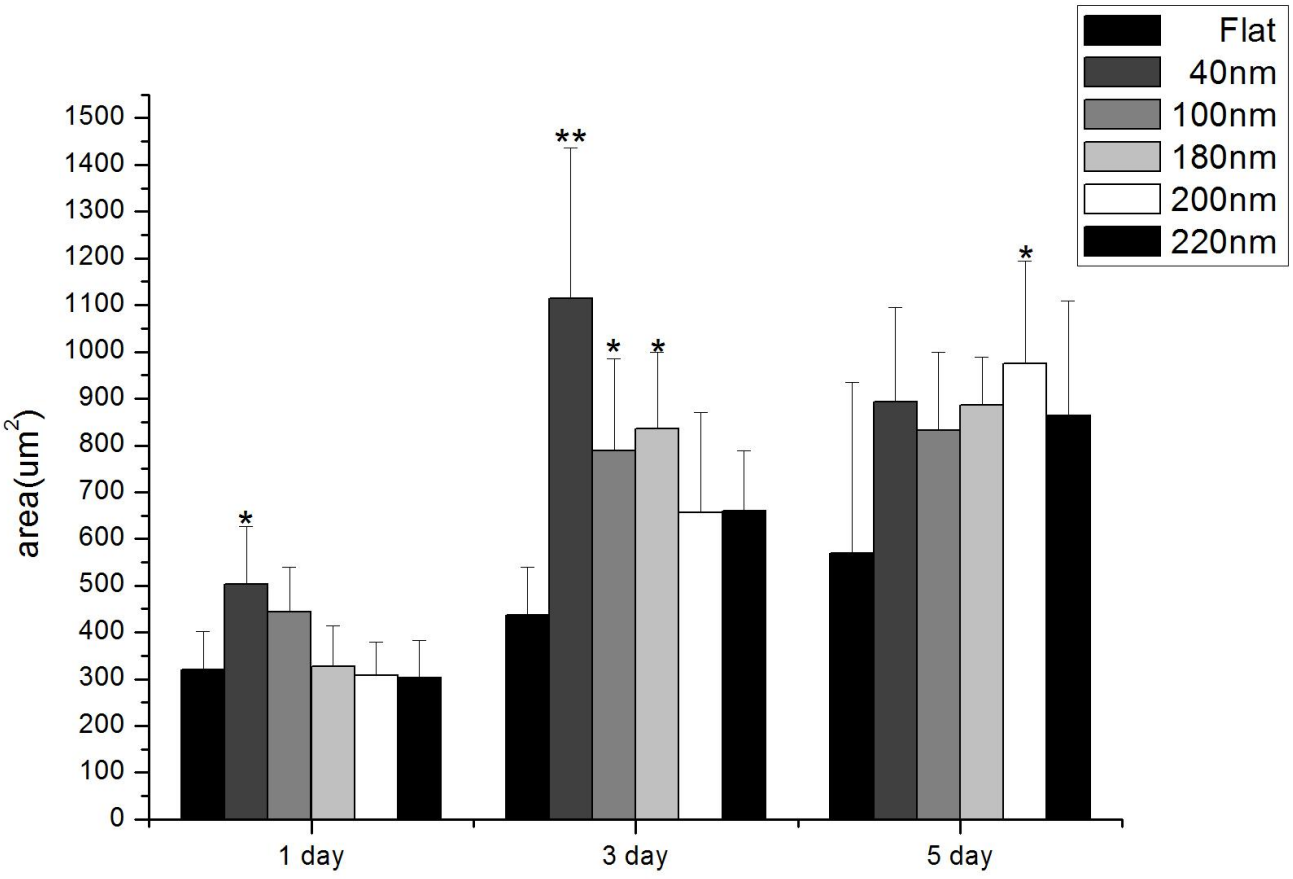

Figure 5.SEM statistics showed cells area. $p<0.005$. The surface area (per cell) seeded on nanopore with control after 1 day, 3 day and 5 day.

2.3Nanotopography modulate cell adhesion and cytoskeleton of MG63

Topography and surface chemistry might share a common pathway to direct cell behavior. Focal adhesions are mediated by cell adhesion through receptor-ligand binding. Number of focal adhesions is the hallmark for cell attachment and can be evaluated by the immunostaining against Vinculin. To evaluate cell adhesion and cytpskeleton reorganization, immunostaonong specific to vinculin and actin filaments was performed (Figure 6,7). Focal adhesion numbers, focal adhesion area per cell, focal adhesion area per focal adhesion contact point and cytoskeleton area were measured (Figure 8).

On day 1, 2-fold increase in focal adhesion number and focal adhesion area per cell for 40-nm compared to flat surface was observed. On day 3, significant increase of focal adhesion number and focal adhesion area per cell for 10-nm and 50-nm was observed. Focal adhesion area per focal adhesion contact point show slight different in compose of surface different and incubating time.

Cytoskeleton organization indicated the growth state of culture cell . On day 1 cell growth on each surface exhibited well define actin

filaments in the cytoplasm, on day 3, increase of actin filament for cell growth on 40nm and 100nm nanopore.

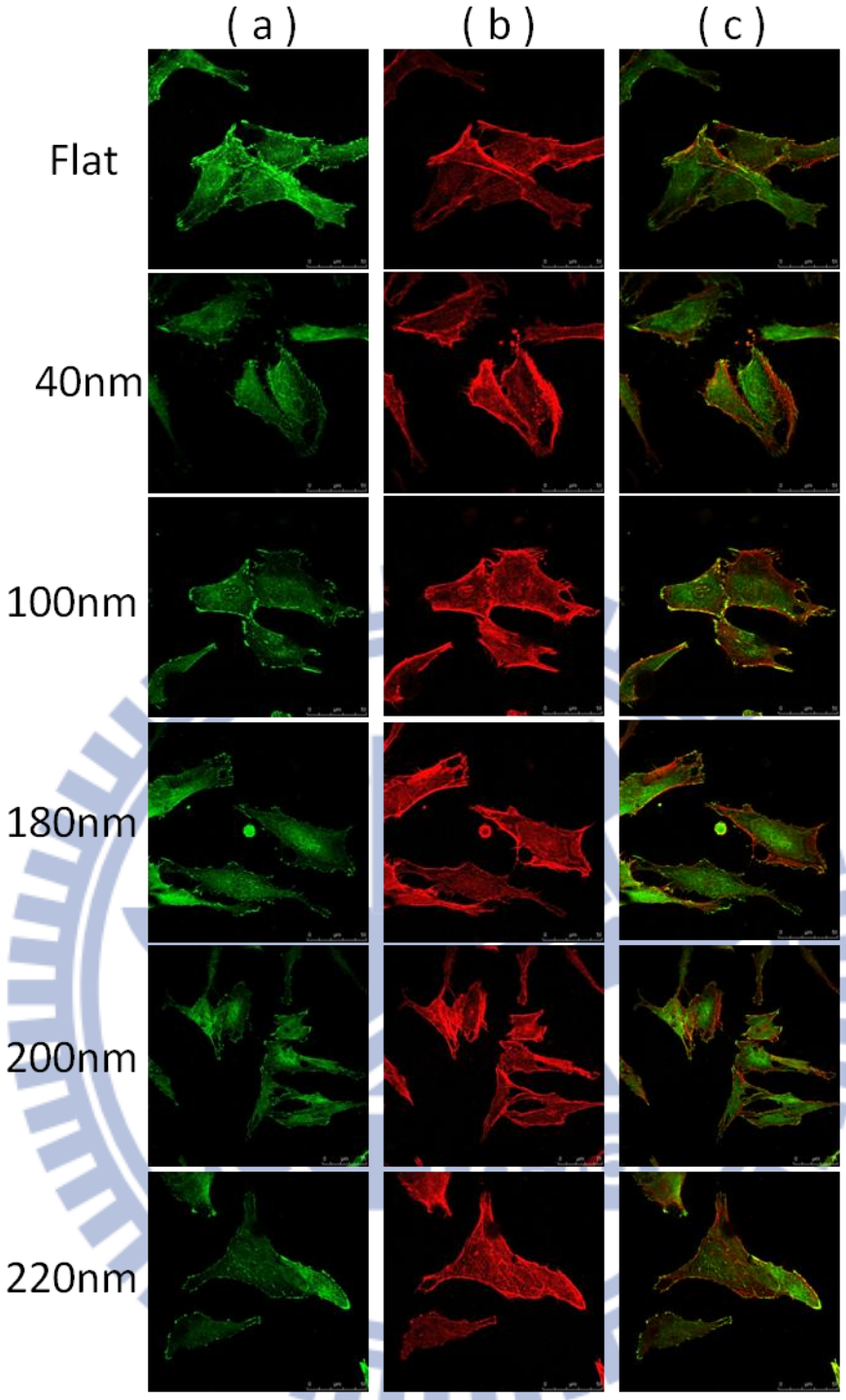

Figure 6.Immunostaoning to show distribution of vinculin (a), actin filament (b) and mergence of vinculin and actin filment(c) in cell culture on 40nm,100nm,180nm,200nm and 220nm nanopore and on flat surface. Cell were seeded on the nanostructure for 1 day before harvest.

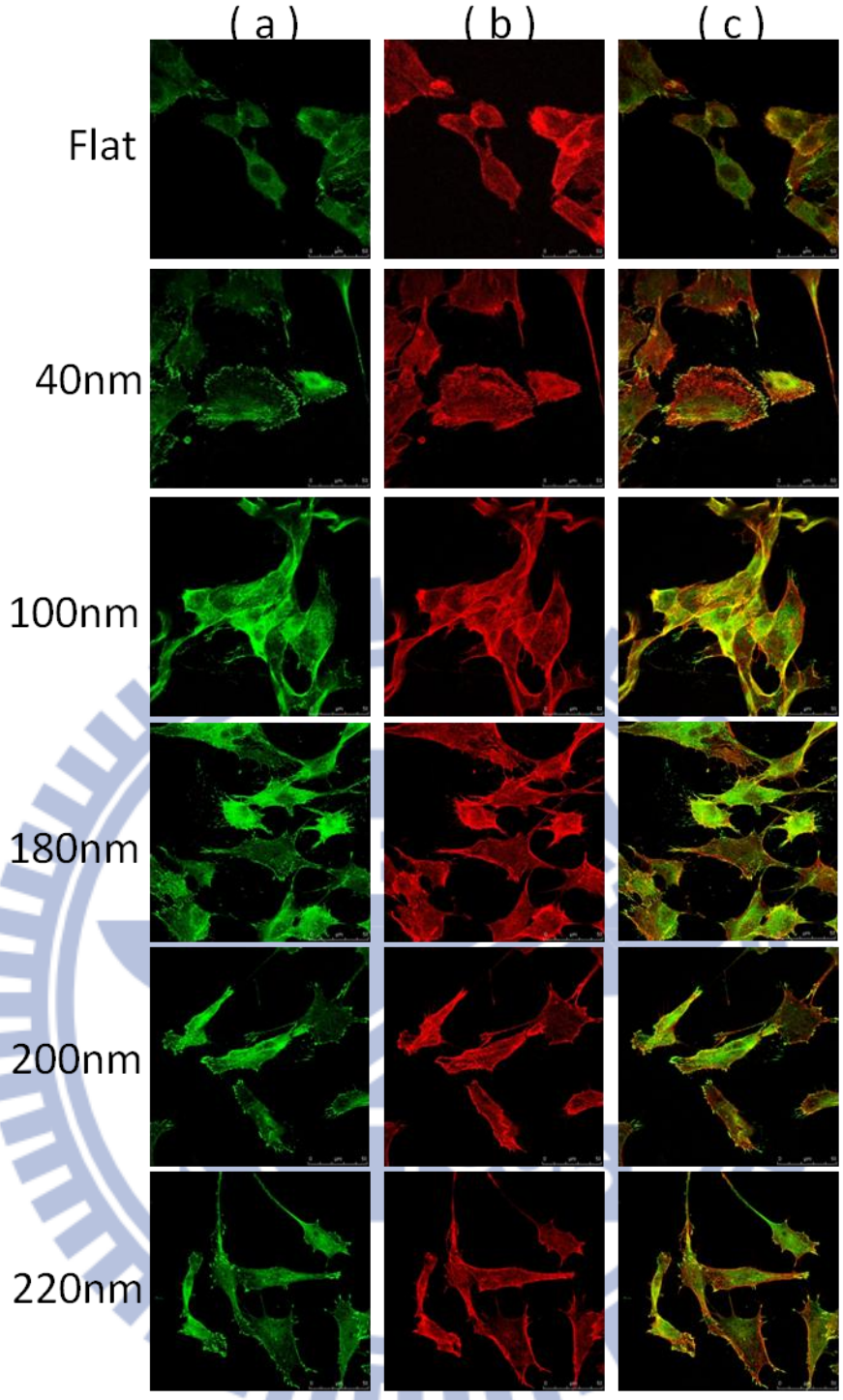

Figure 7.Immunostaoning to show distribution of vinculin (a), actin filament (b) and mergence of vinculin and actin filment(c) in cell culture on 40nm,100nm,180nm,200nm and 220nm nanopore and on flat surface. Cells were seeded on the nanostructure for 3 day before harvest.

(A)

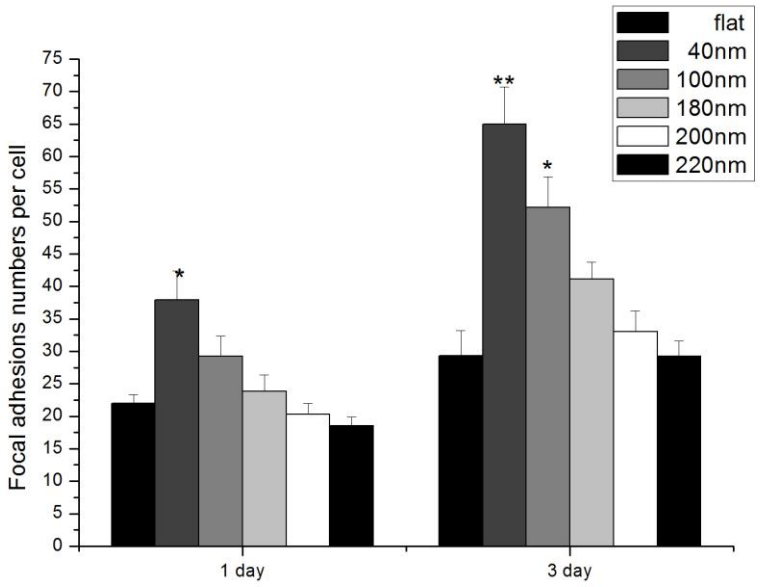
flat
40nm
100nm
180nm
200nm
220nm
Focal adhesions numbers per cell
0
5
10
15
20
25
30
35
40
45
50
55
60
65
70
75
*
**
*
1 day
3 day

(B)

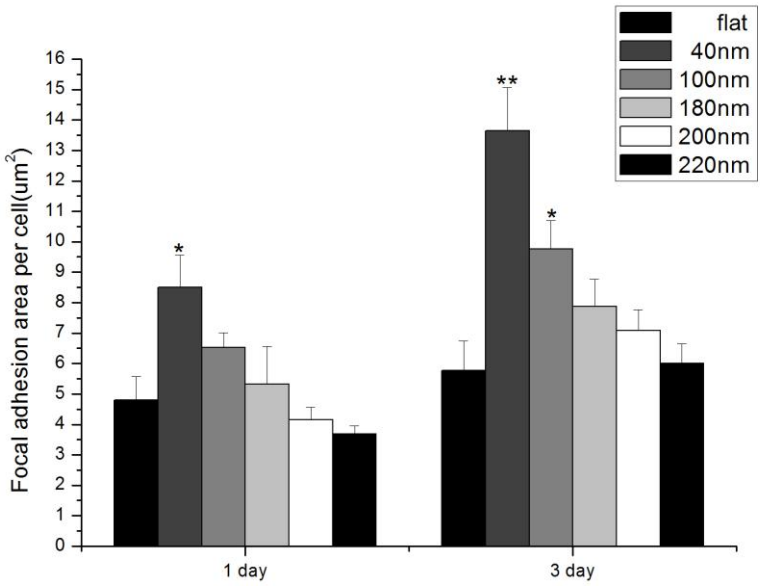
flat
40nm
100nm
180nm
200nm
220nm
Focal adhesion area per cell(um2)
0
1
2
3
4
5
6
7
8
9
10
11
12
13
14
15
16
*
**
*
1 day
3 day

(C)

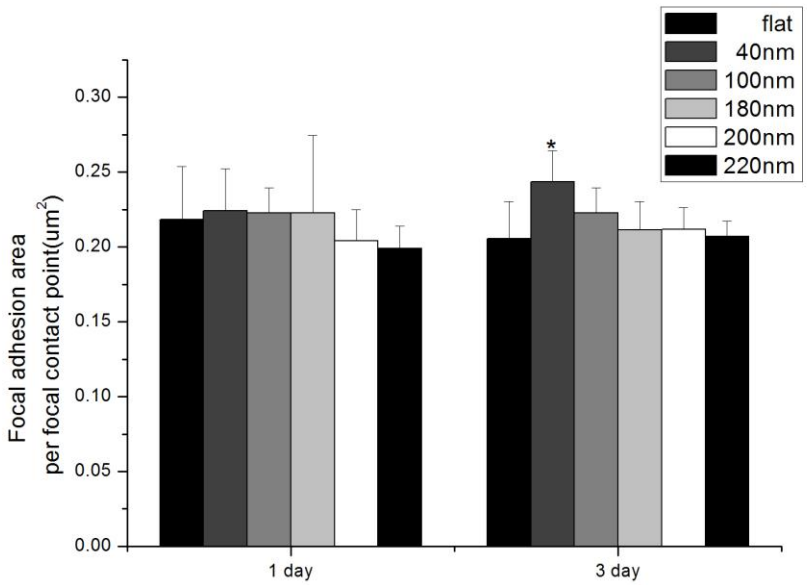

(D)

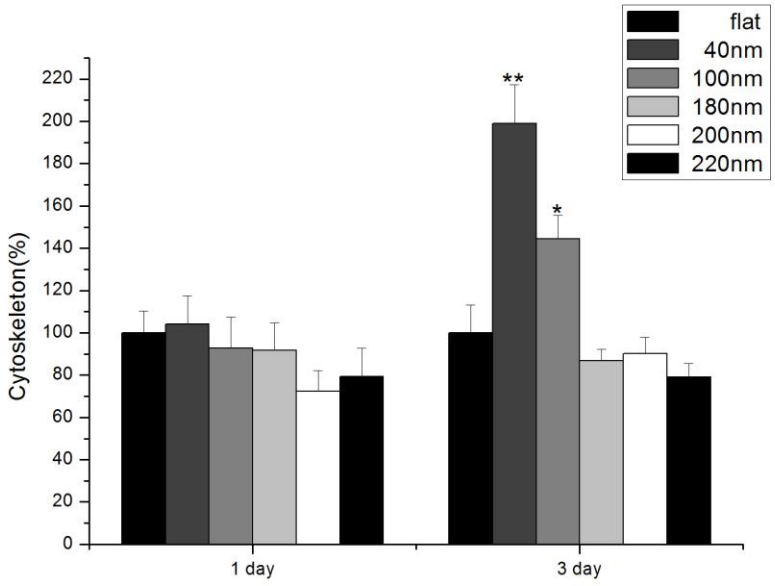

Figure 8. Stastic of focal adhesion numbers, focal adhesion area per cell, focal adhesion area per focal adhesion contact point and cytoskeleton area . MG63 was culture on various nanopore array for 1 day and 3 day. * =p-value , $p<0.005$

2.4Nanostructure modulated mineralization and differentiation of MG63

Mineralization can be assessed by a number of means including fluorescent calcein binding[45], Von Kossa staining[46], and Alizarin red S (ARS) incorporation[47-49]. Both Von Kossa and ARS staining allow simultaneous evaluation of mineral distribution and inspection of fine structures by phase contrast microscopy. ARS staining is particularly versatile in that the dye can be extracted from the stained monolayer and readily assayed. ARS is also used to identify calcium in tissue sections. Matrix mineralization occurs as a consequence of calcium phosphate deposition and can be used as marker for osteogenic differentiation.

For analyzing mineralized nodule formation, osteoblastic cells were cultured for 7 days, 10 days and 14 days and fixed with 10% neutral-buffered formalin and visualized by Alizarin red staining as described previously(Figure 9) and quantification of staining by count red area of osteoblast normalize by cell area.

Figure 10 shows mineralization results of osteoblast after 7, 10, 14 days of culture. The calcium mineral deposition was increasing with increased tube diameter and reached highest on 100 nm nanotubes, then decreasing with increased tube diameter and reached lowest on 220 nanopore after 7 days culture. The calcium mineral deposition of osteoblast cultured on 40nm, 100 nm and 180nm nanopore was higher than the flat, however, the calcium mineral deposition of osteoblast cultured on 200 nm and 220 nm nanopore was lower than the flat. The highest calcium mineral deposition was on 100nm nanopore.

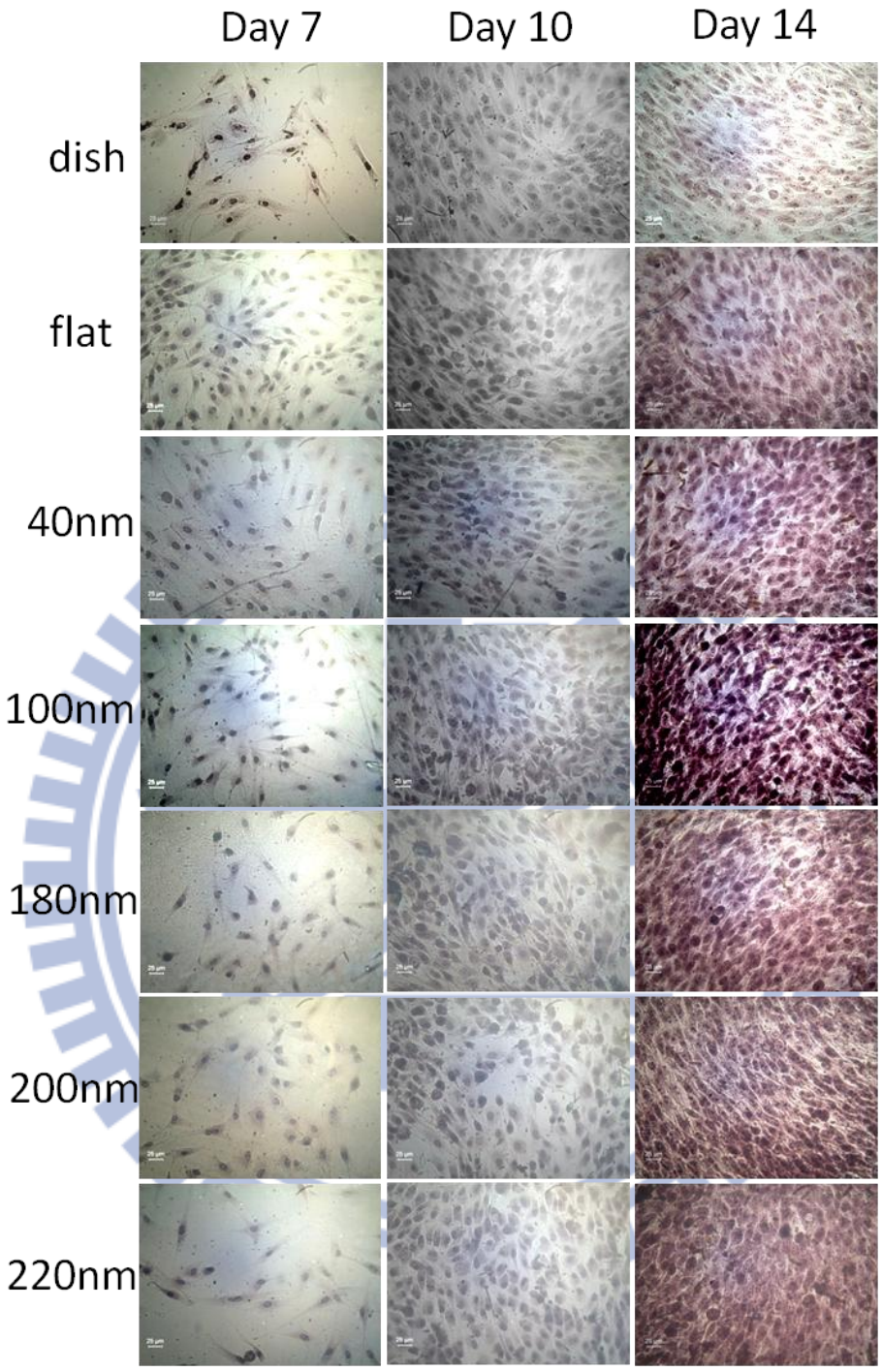

Figure 9.Mineralization of cultured MG63 by Alizarin Red S stain. MG63 cells are seeded on nanopore and growth for 7,10 and 14 days. The mineral was stained as bright red by Alizarin Red S staining.

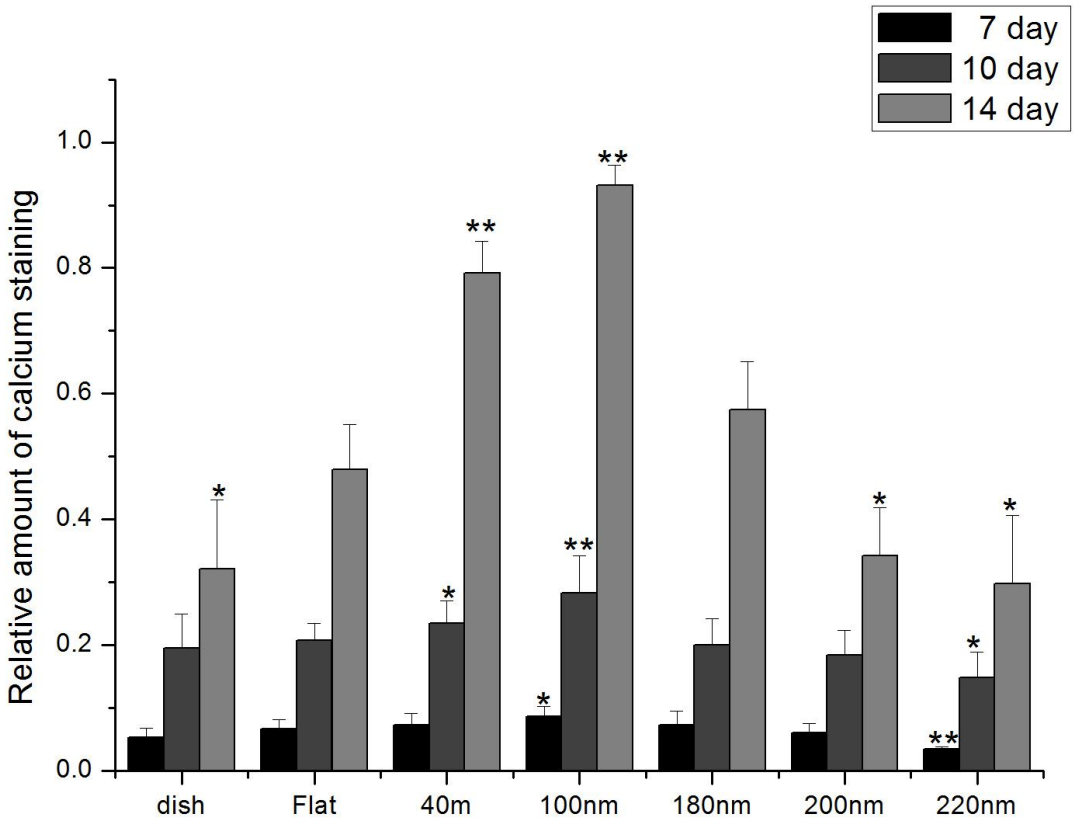

Figure 10.Correlation between mineralization versus size of nanopore. Mg63 is cultured on various sizes of nanopore for 7,10 and 14 days. The Alizarin Red S staining procedure is performed. Mineralization is calculated using the area of bright red. Relative mineralization is calculated relative to flat surface.

The functional activity of the MG63 cells was examined by measuring the ALP activity. ALP activity is an important parameter to access the normal functionality of cells on a surface; hence, the activity was measured for 7, 10 and 14 days of culture(Figure 11).

There were detectable amounts of alkaline phosphatase activity by osteoblasts cultured on all substrates tested in the present study after 7 days. In contrast, alkaline phosphatase activity was significantly greater on 100nm nanopore after 7 days of culture. Alkaline phosphatase activity was also significantly greater when osteoblasts were cultured on 100nm nanopore but less on 200nm and 220nm nanopore than on flat after 10 days. At 14 days of culture, synthesis of alkaline phosphatase by osteoblasts on 40nm, 100nm, 180nm nanopore was 80, 120, and 50% greater than on flat, respectively. The highest alkaline phosphates activity was observed on 100nm nanopoe array.

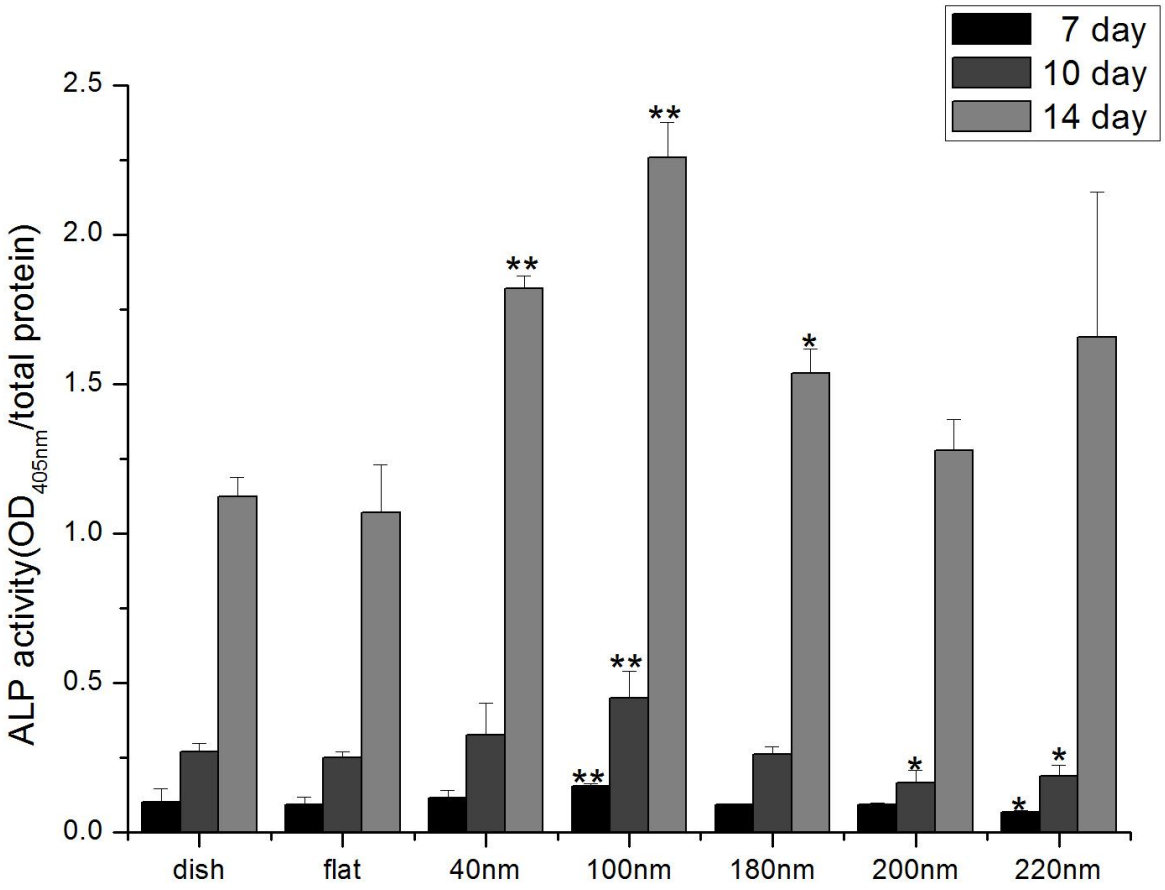

Figure 11. The ALP activity of MG63 osteoblast cultured on different diameter nanopore layers for 7, 10 and 14 day (the ALP activity = absorbance/total protein content): *$p < 0.05$ compared with flat.

III. Conclusions

In this work, we demonstrated that ordered and controlled nanopore of stainless steel by anodization provided a useful model to explore behavior of cells on nanophase regime. The MG63 osteoblast adhere well on 40–100 nm diameter of nanotube layers, but not on 180–220 nm diameter of nanopore layers.

The viability and morphology of cells cultured on different size nanopore layers were significant increasing on 100nm and 40nm nanopore surface, which was mostly caused by the different length and nanometer-scale roughness of the nanopore layers. Furthermore, the ALP activity and mineralization of MG63 osteoblast were obviously suppressed when the tube diameter was 100nm. Thus, further studies are directed towards a response assessment of various cell types cultured on different nanopore layers, which would be helpful for designing better biomaterials.

IV. Reference

1. Diener A, Nebe B, Luthen F, Becker P, Beck U, Neumann HG, et al. Control of focal adhesion dynamics by material surface characteristics. Biomaterials 2005;26(4):383-392.
2. Ionita D, Grecu M, Ungureanu C, Demetrescu I. Modifying the TiAlZr biomaterial surface with coating, for a better anticorrosive and antibacterial performance. Applied Surface Science.
3. Bansiddhi A, Dunand DC. Processing of NiTi foams by transient liquid phase sintering. Journal of Materials Engineering and Performance:1-6.
4. Matsuno H, Yokoyama A, Watari F, Uo M, Kawasaki T. Biocompatibility and osteogenesis of refractory metal implants, titanium, hafnium, niobium, tantalum and rhenium. Biomaterials 2001;22(11):1253-1262.
5. Park SH, Tofighi A, Wang X, Strunk M, Ricketts T, Chang J, et al. Calcium phosphate combination biomaterials as human mesenchymal stem cell delivery vehicles for bone repair. Journal of Biomedical Materials Research Part B: Applied Biomaterials.
6. Nie FL, Wang SG, Wang YB, Wei SC, Zheng YF. Comparative study on corrosion resistance and in vitro biocompatibility of bulk nanocrystalline and microcrystalline biomedical 304 stainless steel. Dental Materials.
7. Martinesi M, Bruni S, Stio M, Treves C, Bacci T, Borgioli F. Biocompatibility evaluation of surface treated AISI 316L austenitic stainless steel in human cell cultures. Journal of Biomedical Materials Research Part A 2007;80(1):131-145.
8. Bordjih K, Jouzeau JY, Mainard D, Payan E, Delagoutte JP, Netter P. Evaluation of the effect of three surface treatments on the biocompatibility of 316L stainless steel using human differentiated cells. Biomaterials 1996;17(5):491-500.
9. Vrouwenvelder WCA, Groot CG, De Groot K. Histological and biochemical evaluation of osteoblasts cultured on bioactive glass, hydroxylapatite, titanium alloy, and stainless steel. Journal of biomedical materials research 1993;27(4):465-475.
10. Malheiro VN, Spear RL, Brooks RA, Markaki AE. Osteoblast and monocyte responses to 444 ferritic stainless steel intended for a Magneto-Mechanically Actuated Fibrous Scaffold. Biomaterials.
11. Davis EM, Li DY, Irvin RT. A peptide-stainless steel reaction that yields a new bioorganic-metal state of matter. Biomaterials.
12. Roguska A, Hiromoto S, Yamamoto A, Wozniak MJ, Pisarek M, Lewandowska M. Collagen immobilization on 316L stainless steel surface with cathodic deposition of calcium phosphate. Applied Surface Science.

13. Gallardo-Moreno AM, Multigner M, Calzado-Martin A, Mendez-Vilas A, Salda a L, Galvan JC, et al. Bacterial adhesion reduction on a biocompatible Si+ ion implanted austenitic stainless steel. Materials Science and Engineering: C.
14. Jamuna-Thevi K, Bakar SA, Ibrahim S, Shahab N. Quantification of silver ion release, in vitro cytotoxicity and antibacterial properties of nanostuctured Ag doped TiO2 coatings on stainless steel deposited by RF magnetron sputtering. Vacuum.
15. Fischer KE, Nagaraj G, Hugh Daniels R, Li E, Cowles VE, Miller JL, et al. Hierarchical nanoengineered surfaces for enhanced cytoadhesion and drug delivery. Biomaterials.
16. Liu Q, Cheng XN, Fei HX. Effects of micro-magnetic field at the surface of 316L and NiTi alloy on blood compatibility. Medical and Biological Engineering and Computing:1-6.
17. Hansson S, Norton M. The relation between surface roughness and interfacial shear strength for bone-anchored implants. A mathematical model* 1. Journal of biomechanics 1999;32(8):829-836.
18. Schwartz Z, Nasazky E, Boyan BD. Surface microtopography regulates osteointegration: the role of implant surface microtopography in osteointegration. The Alpha omegan 2005;98(2):9.
19. Zhao L, Wei Y, Li J, Han Y, Ye R, Zhang Y. Initial osteoblast functions on Ti 5Zr 3Sn 5Mo 15Nb titanium alloy surfaces modified by microarc oxidation. Journal of Biomedical Materials Research Part A;92(2):432-440.
20. Zaveri TD, Dolgova NV, Chu BH, Lee J, Wong J, Lele TP, et al. Contributions of surface topography and cytotoxicity to the macrophage response to zinc oxide nanorods. Biomaterials;31(11):2999-3007.
21. Lee J, Kang BS, Hicks B, Chancellor Jr TF, Chu BH, Wang HT, et al. The control of cell adhesion and viability by zinc oxide nanorods. Biomaterials 2008;29(27):3743-3749.
22. Karuri NW, Liliensiek S, Teixeira AI, Abrams G, Campbell S, Nealey PF, et al. Biological length scale topography enhances cell-substratum adhesion of human corneal epithelial cells. Journal of cell science 2004;117(15):3153.
23. Hung YC, Pan HA, Tai SM, Huang GS. A nanodevice for rapid modulation of proliferation, apoptosis, invasive ability, and cytoskeletal reorganization in cultured cells. Lab Chip;10(9):1189-1198.
24. Park JK, Kim YJ, Yeom J, Jeon JH, Yi GC, Je JH, et al. The Topographic Effect of Zinc Oxide Nanoflowers on Osteoblast Growth and Osseointegration. Advanced Materials.
25. Zhu X, Cui W, Li X, Jin Y. Electrospun fibrous mats with high porosity as potential scaffolds for skin tissue engineering. Biomacromolecules 2008;9(7):1795-1801.
26. Elter P, Sickel F, Ewald A. Nanoscaled periodic surface structures of medical

stainless steel and their effect on osteoblast cells. Acta Biomaterialia 2009;5(5):1468-1473.
27. Liu H, Webster TJ. Nanomedicine for implants: A review of studies and necessary experimental tools. Biomaterials 2007;28(2):354-369.
28. Bjursten LM, Rasmusson L, Oh S, Smith GC, Brammer KS, Jin S. Titanium dioxide nanotubes enhance bone bonding in vivo. Journal of Biomedical Materials Research Part A;92(3):1218-1224.
29. Aninwene GE, Ii CY, Webster TJ. Enhanced osteoblast adhesion to drug-coated anodized nanotubular titanium surfaces. International Journal of Nanomedicine 2008;3(2):257.
30. Park J, Bauer S, von der Mark K, Schmuki P. Nanosize and vitality: TiO2 nanotube diameter directs cell fate. Nano letters 2007;7(6):1686-1691.
31. Popat KC, Eltgroth M, LaTempa TJ, Grimes CA, Desai TA. Decreased Staphylococcus epidermis adhesion and increased osteoblast functionality on antibiotic-loaded titania nanotubes. Biomaterials 2007;28(32):4880-4888.
32. Brammer KS, Oh S, Cobb CJ, Bjursten LM, Heyde H, Jin S. Improved bone-forming functionality on diameter-controlled TiO2 nanotube surface. Acta Biomaterialia 2009;5(8):3215-3223.
33. Vasilev K, Poh Z, Kant K, Chan J, Michelmore A, Losic D. Tailoring the surface functionalities of titania nanotube arrays. Biomaterials;31(3):532-540.
34. Das K, Bose S, Bandyopadhyay A. TiO2 nanotubes on Ti: Influence of nanoscale morphology on bone cell–materials interaction. Journal of Biomedical Materials Research Part A 2009;90(1):225-237.
35. Popat KC, Leoni L, Grimes CA, Desai TA. Influence of engineered titania nanotubular surfaces on bone cells. Biomaterials 2007;28(21):3188-3197.
36. Yao C, Slamovich EB, Webster TJ. Enhanced osteoblast functions on anodized titanium with nanotube like structures. Journal of Biomedical Materials Research Part A 2008;85(1):157-166.
37. Balasundaram G, Yao C, Webster TJ. TiO2 nanotubes functionalized with regions of bone morphogenetic protein 2 increases osteoblast adhesion. Journal of Biomedical Materials Research Part A 2008;84(2):447-453.
38. Peng L, Mendelsohn AD, LaTempa TJ, Yoriya S, Grimes CA, Desai TA. Long-term small molecule and protein elution from TiO2 nanotubes. Nano letters 2009;9(5):1932-1936.
39. Wu H, Liu G, Zhuang Y, Wu D, Zhang H, Yang H, et al. The behavior after intravenous injection in mice of multiwalled carbon nanotube/Fe3O4 hybrid MRI contrast agents. Biomaterials.
40. Smith BS, Johnson T, Popat KC. Dermal fibroblast and epidermal keratinocyte

functionality on titania nanotube arrays. Acta Biomaterialia.
41. Wang N, Li H, Lu W, Li J, Wang J, Zhang Z, et al. Effects of TiO2 nanotubes with different diameters on gene expression and osseointegration of implants in minipigs. Biomaterials.
42. Vashist SK, Zheng D, Pastorin G, Al-Rubeaan K, Luong JHT, Sheu FS. Delivery of drugs and biomolecules using carbon nanotubes. Carbon.
43. Rho JY, Kuhn-Spearing L, Zioupos P. Mechanical properties and the hierarchical structure of bone. Medical engineering & physics 1998;20(2):92-102.
44. Martin F, Del Frari D, Cousty J, Bataillon C. Self-organisation of nanoscaled pores in anodic oxide overlayer on stainless steels. Electrochimica Acta 2009;54(11):3086-3091.
45. Hale LV, Ma YF, Santerre RF. Semi-quantitative fluorescence analysis of calcein binding as a measurement of in vitro mineralization. Calcified Tissue International 2000;67(1):80-84.
46. Tsukimura N, Yamada M, Aita H, Hori N, Yoshino F, Chang-Il Lee M, et al. N-acetyl cysteine (NAC)-mediated detoxification and functionalization of poly (methyl methacrylate) bone cement. Biomaterials 2009;30(20):3378-3389.
47. Gough JE, Jones JR, Hench LL. Nodule formation and mineralisation of human primary osteoblasts cultured on a porous bioactive glass scaffold. Biomaterials 2004;25(11):2039-2046.
48. Abe T, Nomura S, Nakagawa R, Fujimoto M, Kawase I, Naka T. Osteoblast differentiation is impaired in SOCS-1-deficient mice. Journal of bone and mineral metabolism 2006;24(4):283-290.
49. Taubenberger AV, Woodruff MA, Bai H, Muller DJ, Hutmacher DW. The effect of unlocking RGD-motifs in collagen I on pre-osteoblast adhesion and differentiation. Biomaterials;31(10):2827-2835.